Frontiers of Information Technology & Electronic Engineering
www.jzus.zju.edu.cn; engineering.cae.cn; www.springerlink.com
ISSN 2095-9184 (print); ISSN 2095-9230 (online)
E-mail: jzus@zju.edu.cn

Design of a wideband symmetric large back-off range Doherty power amplifier based on impedance and phase hybrid optimization*

Zhongpeng NI[1], Jing XIA[†‡1], Xinyu ZHOU[2], Wa KONG[1], Wence ZHANG[1], Xiaowei ZHU[3]

[1]*School of Computer Science and Communication Engineering, Jiangsu University, Zhenjiang 212013, China*

[2]*Department of Electrical and Electronic Engineering, The Hong Kong Polytechnic University, Hong Kong 999077, China*

[3]*State Key Laboratory of Millimeter Waves, Southeast University, Nanjing 210096, China*

[†]E-mail: jingxia@ujs.edu.cn

Received Jan. 29, 2024; Revision accepted May 27, 2024; Crosschecked Nov. 13, 2024; Published online Dec. 26, 2024

Abstract: The present paper proposes an optimization design method for the Doherty output matching network (OMN) using impedance–phase hybrid objective function constraints, which possesses the capability of enhancing the efficiency consistency of the Doherty power amplifier (DPA) using integrated enhancing reactance (IER) during the back-off power (BOP) range. By calculating the desired reactance for an extended BOP range and combining it with the two-impedance matching method, the S-parameters of the OMN are obtained. Meanwhile, the impedance and phase constraints of the OMN are proposed to narrow the distribution range of the IER. Furthermore, a fragment-type structure is employed in the OMN optimization so as to enhance the flexibility of the circuit optimization design. To validate the proposed method, a 1.7–2.5 GHz symmetric DPA with a large BOP range was designed and fabricated. Measurement results demonstrate that across the entire operating frequency band, the saturated output power is >44 dBm, and the efficiency ranges from 45% to 55% at a 9-dB BOP.

Key words: Back-off power range; Doherty power amplifier; Fragment-type structure; Impedance–phase hybrid function

https://doi.org/10.1631/FITEE.2400066 **CLC number:** TN722

1 Introduction

To fulfill the requirements of high data rates and greater spectral efficiency, complex modulation techniques are often employed in modern wireless communication systems, resulting in modulation signals having a higher peak-to-average power ratio (PAPR) (Liu et al., 2020). The power amplifier, as a critical component of wireless communication systems, has received widespread attention from researchers (Yang et al., 2019; Li M et al., 2022; Wang et al., 2022; Cui et al., 2023; Dai et al., 2024; Ren et al., 2024; Yao et al., 2024). Several techniques have been proposed to address the challenges posed by high PAPR, such as the out-phasing amplifier (Chung et al., 2018), the envelope tracking amplifier (Asbeck and Popovic, 2016), and the Doherty power amplifier (DPA) (Doherty, 1936). Among these, the DPA has gained significant attention due to its simple structure and excellent performance at high back-off power (BOP) levels. However, conventional symmetrical DPAs achieve efficiency enhancement only at 6-dB BOP within a narrow operating frequency band, which is insufficient to meet the

‡ Corresponding author

* Project supported by the National Natural Science Foundation of China (Nos. 62171204, 62001192, and 62171129)

ORCID: Jing XIA, https://orcid.org/0000-0001-6255-9297

growing communication demands.

To improve the BOP range, various complex architectures have been proposed, including multi-stage (Zhou H et al., 2022), multi-way (Chen et al., 2018), and asymmetric (Xu et al., 2021; Roychowdhury and Kitchen, 2022; Li MY et al., 2023) DPAs. However, these methods involve higher design complexity, requiring a trade-off between the cost and power utilization factors. Consequently, extensive research has focused on extending the operating bandwidth and efficiency-enhancement range of symmetric DPAs. Several techniques, including transformer-less load-modulated power amplifiers (Akbarpour et al., 2012; Zhou LH et al., 2023), integrated compensating reactance (Xia et al., 2016), continuous class mode (Shi et al., 2018), improved load modulation networks (Nan et al., 2021), and post-matching networks (Pang et al., 2015; Lyu et al., 2023), have been observed to achieve high-efficient operation over a wide bandwidth. Furthermore, methods such as the three-port harmonic injection networks (Zhou XY et al., 2022), co-design of three matching sub-networks (Li C et al., 2020), phase compensation (Ruhul Hasin and Kitchen, 2019; Zhang JR et al., 2023), complex combining load (Fang and Cheng, 2014; Choi et al., 2021), and non-infinite auxiliary output impedance (Özen et al., 2016; Shi et al., 2017; Xiao et al., 2021) have been proposed to extend the efficiency enhancement range of DPAs. In Kong et al. (2018), a method based on integrated enhancing reactance (IER) was proposed to expand the BOP range. This is unlike the method that uses a post-matching network to provide a complex load impedance. When the DPA operates in a back-off state, the proposed DPA uses the $\mathrm{j}X_{\mathrm{IER}}$ provided by the auxiliary amplifier to extend the BOP range. When the DPA operates in saturation, the modulation of the DPA during saturation is not affected, which greatly reduces the design complexity of the output matching network (OMN). However, the DPA designed using this method does not consider the influence of phase dispersion in the OMN on the IER within a wide frequency band, resulting in significant efficiency variations between high and low frequencies at the BOP and limiting its ability to achieve a wider bandwidth. Therefore, if a more compact IER can be achieved through appropriate phase constraints, then the DPA using IER still has potential for enhancing the bandwidth.

Moreover, conventional power amplifier designs commonly use regular microstrip circuit structures, which limits the feasibility of the circuit optimization. To overcome these limitations and further enhance the power amplifier performance, a fragment-type microstrip circuit has been used in the power amplifier design. It demonstrates a flexible layout structure that effectively reduces phase dispersion and offers greater design flexibility (Xia et al., 2022; Karahan et al., 2023; Kong et al., 2024).

In the present paper, an integrated optimization approach for impedance and phase in the broadband symmetric DPA is proposed. First, the phase required by the auxiliary output matching network ($\mathrm{OMN_A}$) is thoroughly analyzed and then combined with the target impedance. Second, a flexible fragment-type structure of microstrip circuits is employed for the optimization. Compared with conventional designs, the proposed method significantly mitigates phase dispersion across a wide frequency band, enabling wideband high-efficiency operation of the DPA under large back-off conditions.

2 Theoretical analysis of enhancing the BOP range

The schematic of a DPA based on the IER is illustrated in Fig. 1. It comprises an input power divider, offset lines, main and auxiliary amplifiers, and a post-matching network. The load impedances of the main amplifier at the current source plane, package plane, and modulation point, respectively, when the DPA operates in the saturation state, are represented as $Z_{\mathrm{M}i,\mathrm{sat}}$, $Z_{\mathrm{M,sat}}$, and $Z_{\mathrm{M1,sat}}$. Similarly, the load impedances of the auxiliary amplifier at the package plane and modulation point are denoted as $Z_{\mathrm{A,sat}}$ and $Z_{\mathrm{A1,sat}}$, respectively. In the back-off state, the corresponding load impedances become $Z_{\mathrm{M}i,\mathrm{bop}}$, $Z_{\mathrm{M,bop}}$, $Z_{\mathrm{M1,bop}}$, $Z_{\mathrm{A,out}}$, and $Z_{\mathrm{A1,out}}$, where $Z_{\mathrm{A1,out}}$ can be used as the IER ($\mathrm{j}X_{\mathrm{IER}}$). Γ_i and Γ_1 represent the reflection coefficients at the current source plane and modulation point, respectively. Unlike conventional DPAs, the IER ($\mathrm{j}X_{\mathrm{IER}}$) is introduced in the DPA using IER in the back-off state to expand the range of the efficiency enhancement. In previous designs, the impact of IER distribution on bandwidth was not fully considered, resulting in a relatively narrow bandwidth. This study achieves a more focused IER distribution and effectively expands the

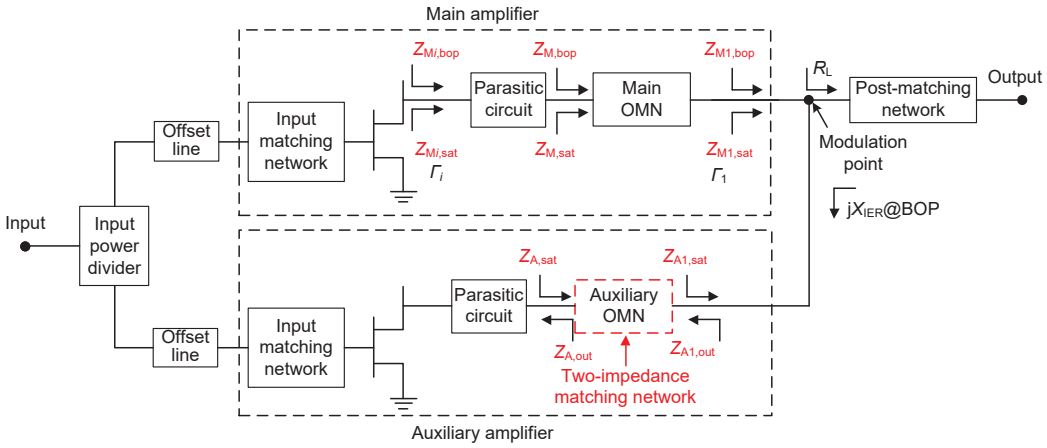

Fig. 1 Schematic of the proposed DPA (DPA: Doherty power amplifier; OMN: output matching network; BOP: back-off power)

bandwidth by controlling the phase to reduce phase dispersion.

2.1 Calculation of IER

The BOP range of a DPA can be calculated based on the output power in both the saturation and back-off states (Fang and Cheng, 2014). Given that a symmetric DPA design is employed, the power ratio of the auxiliary amplifier to the main amplifier (α) is set to 1 and the dynamic load span ratio β is as depicted in Eq. (2).

$$\begin{aligned}\mathrm{BOP} &= 10\lg\left(\frac{P_{\mathrm{sat}}}{P_{\mathrm{bop}}}\right)\\ &= 10\lg\left[(1+\alpha)\,\beta\right]\\ &= 10\lg\beta + 3\,(\mathrm{dB})\,.\end{aligned} \tag{1}$$

$$\beta = \frac{P_{\mathrm{M,sat}}}{P_{\mathrm{M,bop}}} = \frac{Z_{\mathrm{M}i,\mathrm{bop}}}{Z_{\mathrm{M,sat}}}. \tag{2}$$

Considering that the impedances at the current source plane are purely resistive, the relationship between the magnitude of the reflection coefficient and the load impedance at the current source plane is shown in Eq. (3). Then, the relationship between the BOP range and the reflection coefficient at the current source plane can be further derived based on the reflection coefficient calculation formula, as specifically shown in Eq. (4). Theoretically, the expansion of the BOP range can be achieved by increasing the magnitude of the reflection coefficient Γ_i.

$$|\Gamma_i| = \frac{Z_{\mathrm{M}i,\mathrm{bop}} - Z_{\mathrm{M}i,\mathrm{sat}}}{Z_{\mathrm{M}i,\mathrm{sat}} + Z_{\mathrm{M}i,\mathrm{bop}}}. \tag{3}$$

$$\begin{aligned}\mathrm{BOP} &= 10\lg\left(\frac{Z_{\mathrm{M}i,\mathrm{bop}}}{Z_{\mathrm{M}i,\mathrm{sat}}}\right) + 3\ (\mathrm{dB})\\ &= 10\lg\left(\frac{1+|\Gamma_i|}{1-|\Gamma_i|}\right) + 3\ (\mathrm{dB}).\end{aligned} \tag{4}$$

The parasitic parameter network and the OMN can be theoretically considered lossless. Based on the microwave theory, the relationship between the magnitude of the reflection coefficients Γ_i and Γ_1 can be obtained in Eq. (5). Therefore, the BOP range of the DPA can be expressed in the form of Eq. (6).

$$|\,\Gamma_i\,| = |\,\Gamma_1\,|\,. \tag{5}$$

$$\mathrm{BOP} = 10\lg\left(\frac{1+|\,\Gamma_1\,|}{1-|\,\Gamma_1\,|}\right) + 3\ (\mathrm{dB}). \tag{6}$$

Therefore, by adjusting the magnitude of Γ_1, the BOP range of the DPA can be significantly expanded. Fang and Cheng (2014) proposed using a complex combined load to enhance the BOP range of DPA. However, this method is difficult to achieve impedance matching when the DPA operates in a saturation state, which inevitably results in a decrease in the output power and efficiency. A method based on the IER was proposed by Kong et al. (2018), which does not affect the load modulation at saturation, thus simplifying the design complexity of the main output matching network ($\mathrm{OMN_M}$). In the back-off state, an IER $\mathrm{j}X_{\mathrm{IER}}$ is generated by the auxiliary amplifier in the DPA using IER to expand the BOP range. As a result, the impedance of the main amplifier $Z_{\mathrm{M1,bop}}$ is no longer R_{L} but a parallel combination of R_{L} and $\mathrm{j}X_{\mathrm{IER}}$. It is worth noting that when the amplifier operates in saturation,

the $\mathrm{j}X_{\mathrm{IER}}$ will not affect the characteristics of DPA. Therefore, the saturated impedance of the main amplifier $Z_{\mathrm{M1,sat}}$ equals $2R_{\mathrm{L}}$, which is purely resistive. Hence, the reflection coefficient at the modulation point can be expressed as follows:

$$\begin{aligned}\Gamma_1 &= \frac{R_{\mathrm{L}}//\mathrm{j}X_{\mathrm{IER}} - Z_{\mathrm{M1,sat}}}{R_{\mathrm{L}}//\mathrm{j}X_{\mathrm{IER}} + Z^*_{\mathrm{M1,sat}}} \\ &= \frac{R_{\mathrm{L}}//\mathrm{j}X_{\mathrm{IER}} - 2R_{\mathrm{L}}}{R_{\mathrm{L}}//\mathrm{j}X_{\mathrm{IER}} + 2R_{\mathrm{L}}},\end{aligned} \tag{7}$$

where "//" represents the parallel operation and "*" represents the conjugate.

By rearranging Eq. (7), the required IER $\mathrm{j}X_{\mathrm{IER}}$ for achieving large BOP range can be obtained as follows:

$$\mathrm{j}X_{\mathrm{IER}} = \frac{-2R_{\mathrm{L}}\left(1+\Gamma_1\right)}{1+3\Gamma_1}. \tag{8}$$

2.2 Impedance–phase hybrid objective function

In the design process of the DPA using IER, it is necessary to appropriately design $\mathrm{OMN_A}$ to achieve the desired IER and expand the BOP range. Based on the calculated IER from Section 2.1 and considering the impedance matching requirements of $\mathrm{OMN_A}$ in both the back-off and saturation states, the transformations from $Z_{\mathrm{A,out}}$ to the desired $Z_{\mathrm{A1,out}}$ (IER $\mathrm{j}X_{\mathrm{IER}}$) and from $Z_{\mathrm{A,sat}}$ to the desired $Z_{\mathrm{A1,sat}}$ need to be achieved, as shown in Fig. 1. The S-parameters of $\mathrm{OMN_A}$ can be obtained and used for the optimization design based on the two-impedance matching method (Xia et al., 2016). However, the phase differences in S_{21} of $\mathrm{OMN_A}$ over the entire frequency range have a significant impact on the amplifier's bandwidth. For example, in the DPA designed by Kong et al. (2018), the efficiency difference at 9-dB BOP over the entire frequency band reaches 10%, indicating poor efficiency consistency and affecting the broadband performance. This is because complex OMNs are often used in the broadband DPA designs to achieve the required impedance–transformation ratio. Unfortunately, these complex OMNs may cause sharp phase variations within the operating frequency band, thereby reducing the efficiency consistency during the DPA BOP range. Therefore, an integrated approach involving impedance and phase constraints is proposed to make the distribution of the required IER more concentrated, thereby enhancing the efficiency consistency of the DPA using IER.

First, for the load impedance, the optimal value Z_{opt} is obtained through load-pull simulations. The absolute difference between the real and imaginary parts of the impedance Z_{L} achieved by the OMN and the target impedance Z_{opt} is calculated, and it serves as the impedance optimization objective function. Second, based on the desired values of the IER, the required phase θ_{opt} for the OMN can be calculated using the two-impedance matching method. The absolute difference between the phase θ of the OMN and the desired phase θ_{opt} is used as the phase optimization objective function. Finally, by combining the impedance and phase constraints, the following hybrid objective function can be derived:

$$\begin{aligned}&F_{Z\_\theta}(Z_{\mathrm{L}},\theta) \\ =&\max\left(\left|R_{\mathrm{L}}-R_{\mathrm{opt}}\right|+\left|X_{\mathrm{L}}-X_{\mathrm{opt}}\right|,\left|\theta-\theta_{\mathrm{opt}}\right|\right),\end{aligned} \tag{9}$$

where the objective function F_{Z_θ} is the maximum value between the impedance difference and the phase difference, and R and X correspond to the real and imaginary parts respectively. When $F_{Z\_\theta}<1$, it indicates that the design requirements of the impedance and phase have been satisfied.

3 Design and simulation

A fragment-type structure for OMN is proposed for optimization to minimize the IER dispersion caused by the phase difference between high and low frequencies in the matching network, thereby achieving consistent efficiency during the operation of BOP. The following subsections provide a detailed analysis and design methodology for this approach.

3.1 Optimization strategy based on the impedance–phase hybrid objective function

$\mathrm{OMN_A}$ is optimized by using the following strategy within the desired frequency range of 1.7–2.5 GHz.

For the high frequency, the optimal load impedance at 2.5 GHz at saturation is determined to be (14+j1) Ω through load-pull simulation. Based on Eq. (8), when R_{L} is 28 Ω, $\mathrm{j}X_{\mathrm{IER}}$ can be calculated as −j30 Ω. By using the two-impedance matching method (Xia et al., 2016), the corresponding phase of $\mathrm{OMN_A}$ at 2.5 GHz is determined to be −215°. Therefore, the optimization objective function for

$\mathrm{OMN_A}$ at the high frequency is given as follows:

$$F_{Z\_\theta\_2.5\mathrm{GHz}}(Z_\mathrm{L},\theta) = \max(|R_\mathrm{L}-14|+|X_\mathrm{L}-1|,|\theta+215|). \tag{10}$$

For the center and low frequencies, it is difficult to precisely determine the values of the optimal load impedance and phase required. To address this issue, an impedance constraint circle is employed for the impedance target, and a phase balancing strategy is used to minimize the phase difference. As shown in Fig. 2a, an impedance constraint circle tangent to the desired impedance region is constructed with the center of Z_opt and a radius of r_T. Z_opt represents the optimal load impedance and Z_T is an impedance on the desired impedance region. Thus, r_T can be calculated by Eq. (11). During the optimization process, the impedance objective function is defined based on the relative position relationship of impedance Z_L and the optimal load impedance Z_opt, as shown in Eq. (12). If $F_Z(Z_\mathrm{L})<1$, the load impedance Z_L is within the impedance constraint circle corresponding to the desired impedance region.

$$r_\mathrm{T}=\left|\frac{Z_\mathrm{T}-Z_\mathrm{opt}}{Z_\mathrm{T}+Z_\mathrm{opt}^*}\right|. \tag{11}$$

$$F_Z(Z_\mathrm{L})=\frac{1}{r_\mathrm{T}}\left|\frac{Z_\mathrm{L}-Z_\mathrm{opt}}{Z_\mathrm{L}+Z_\mathrm{opt}^*}\right|. \tag{12}$$

Additionally, as depicted in Fig. 2b, the phase objective function is formulated by evaluating the phase differences between the low–center and center–high frequencies, as follows:

$$F_\theta(\theta)=(\theta_\mathrm{l}-\theta_\mathrm{h})/\mathrm{PD_{opt}}, \tag{13}$$

where θ_l and θ_h represent the phases of the lower and higher frequencies, respectively, and $\mathrm{PD_{opt}}$ denotes the target phase difference.

According to the load-pull results, the optimal load impedance Z_opt at 2.1 and 1.7 GHz is (30+j0) Ω and (25+j3) Ω, respectively. Similarly, the corresponding values for Z_T are (36+j20) Ω and (30+j20) Ω. To increase the consistency of amplifier efficiency during BOP range, it is desired to have a phase difference of <25° between 1.7 and 2.1 GHz, as well as between 2.1 and 2.5 GHz. Therefore, the optimization objective functions for $\mathrm{OMN_A}$ at the center and low frequencies can be defined in Eqs. (14) and (15), respectively. When the value of the optimized objective function is <1, it indicates that the optimized load impedance and phase meet the design requirements.

$$F_{Z\_\theta\_2.1\mathrm{GHz}}(Z_\mathrm{L},\theta) = \max(F_{Z\_2.1\mathrm{GHz}}(Z_\mathrm{L}),F_{\theta\_2.1\mathrm{GHz}}(\theta)). \tag{14}$$

$$F_{Z\_\theta\_1.7\mathrm{GHz}}(Z_\mathrm{L},\theta) = \max(F_{Z\_1.7\mathrm{GHz}}(Z_\mathrm{L}),F_{\theta\_1.7\mathrm{GHz}}(\theta)). \tag{15}$$

3.2 Design of $\mathrm{OMN_A}$

Based on the previously mentioned optimization strategy, a fragment-type structure is selected for the $\mathrm{OMN_A}$ design to reduce the phase dispersion. To ensure sufficient design freedom for optimization, the $\mathrm{OMN_A}$ to be designed is depicted in Fig. 3. Appropriately structured microstrip lines are pre-selected, and regions sensitive to impedance and phase are optimized using fragment-type structures.

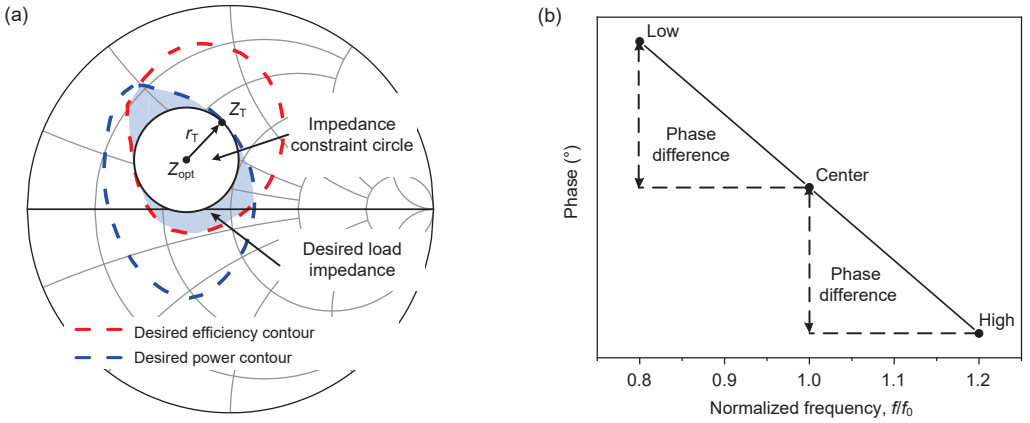

Fig. 2 Illustration of the objective functions for center- and low-frequency optimization: (a) impedance; (b) phase. References to color refer to the online version of this figure

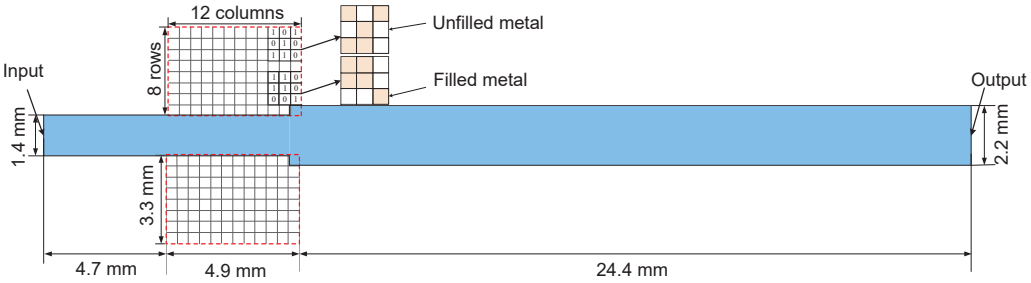

Fig. 3 Structure of the fragment-type auxiliary output matching network (OMN_A)

If the requirements are not met, adjustments will continue on the regularly structured microstrip lines and the fragment-type regions until the optimization requirements are satisfied. After multiple attempts, a region with 16 rows and 12 columns was selected for optimization. Unlike conventional regular structures, which contain only length and width as optimization parameters, the fragment-type structure consists of a set of binary codes, where "1" represents a grid filled with metal and "0" indicates that it is not filled. Theoretically, the matching network structure shown in Fig. 3 has 2^{192} possibilities.

In this study, a multi-objective evolutionary algorithm based on decomposition (MOEA/D) is used to generate the design parameters of the fragment-type structure for OMN_A (Zhang QF and Li, 2007). The design parameters are optimized using three objective functions corresponding to high, center, and low frequencies. The algorithm uses a population size of 40 and performs 50 optimization iterations. This optimization method effectively integrates MATLAB and electromagnetic simulation software through a VB script. First, design variables are randomly generated in MATLAB. Second, these variables are transmitted to High Frequency Structure Simulator (HFSS) for modeling and simulation using a VB script. Finally, the fitness value is calculated based on the proposed impedance–phase hybrid objective function, and MOEA/D is employed for iterative updates to find the optimal design variables. Fig. 4 provides a detailed illustration of the steps in the optimization process.

The convergence curves for the different structures are depicted in Fig. 5. It is evident that the fragment-type structure exhibits superior convergence properties in fitness values for objectives 2 and 3 (at frequencies of 2.1 and 1.7 GHz, respectively), compared to the conventional regular structure. However, at the frequency of 2.5 GHz, which corresponds to objective 1, the regular structure shows a lower fitness value. According to the fitness calculation formula defined previously for objective 1, a fitness value <1 is considered to meet the optimization requirements. Thus, although the performance of the fragment-type structure in terms of fitness for objective 1 is not as good as that of the conventional structure, it still meets the expected optimization objectives.

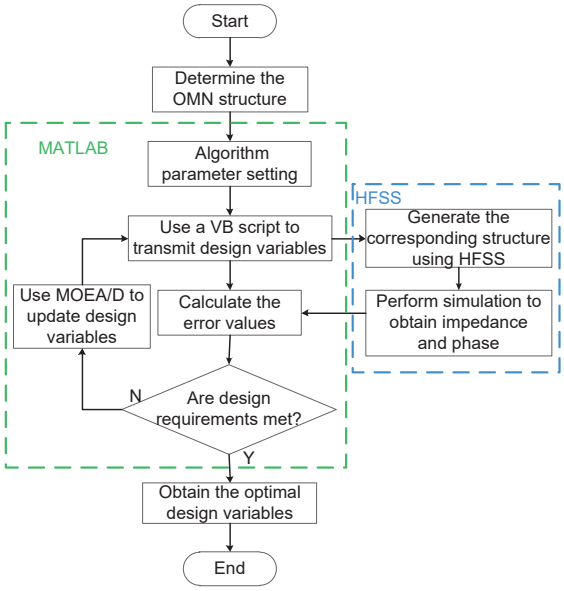

Fig. 4 Design flowchart of the proposed method (OMN: output matching network; MOEA/D: multi-objective evolutionary algorithm based on decomposition; HFSS: High Frequency Structure Simulator)

Fig. 6 presents the simulated phase values and load impedances of OMN_A. It can be observed that the load impedance $Z_{A,sat}$ satisfies the impedance requirement. Furthermore, the range of IER ($Z_{A1,out}$) for the fragment-type structure spans from $-j30\,\Omega$ to

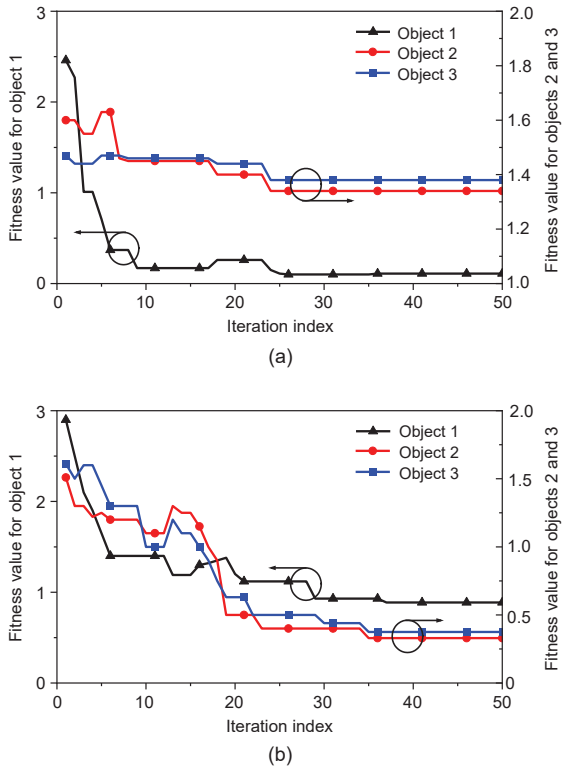

Fig. 5 Fitness value of the objective functions in the optimization process: (a) regular structure; (b) fragment-type structure

−j115 Ω. For comparison, the impedance and phase results from the regular structure are provided. The comparison results demonstrate that the fragment-type structure possesses greater optimization flexibility in terms of impedance matching and phase control, which can improve the consistency of efficiency in the wideband large BOP range DPA.

3.3 Design and simulation of the proposed DPA

To validate the proposed optimization method, a large BOP range DPA is designed using Wolfspeed CGH40010F GaN HEMT for the frequency range of 1.7–2.5 GHz. To achieve the power ratio of 1, after evaluation using load-pull simulations, the drain voltages for the main and auxiliary amplifiers are set to 24 V and 28 V with the gate voltages of −3 V and −6 V, respectively. The impedance constraint circle method combined with the fragment-type structure is also employed to design OMN_M, as shown in Fig. 6a along with the impedance simulation results. An Anaren X3C22E1-03S 3-dB 90° hybrid coupler is

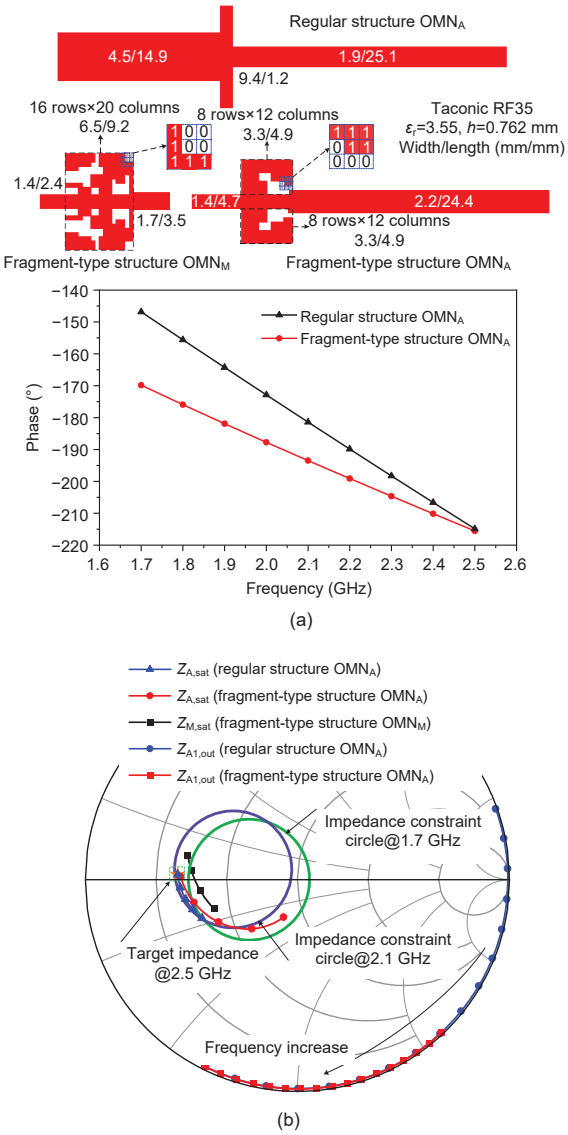

Fig. 6 The optimized output matching network (OMN) and simulation results in the 1.7–2.5 GHz frequency band: (a) phase; (b) impedance

selected as the input power divider. The complete schematic of the proposed DPA is given in Fig. 7.

The simulated drain efficiency (DE) versus output power in the frequency range of 1.7–2.5 GHz is shown in Fig. 8a to verify the performance of the designed fragment-type structure DPA. It is shown that the DE at 9-dB BOP and the saturation is 48%–58% and 55%–74%, respectively. The efficiency at a 9-dB BOP is further illustrated in Fig. 8b, which presents the relationship between DE and frequency, confirming the effectiveness of the fragment-type structure.

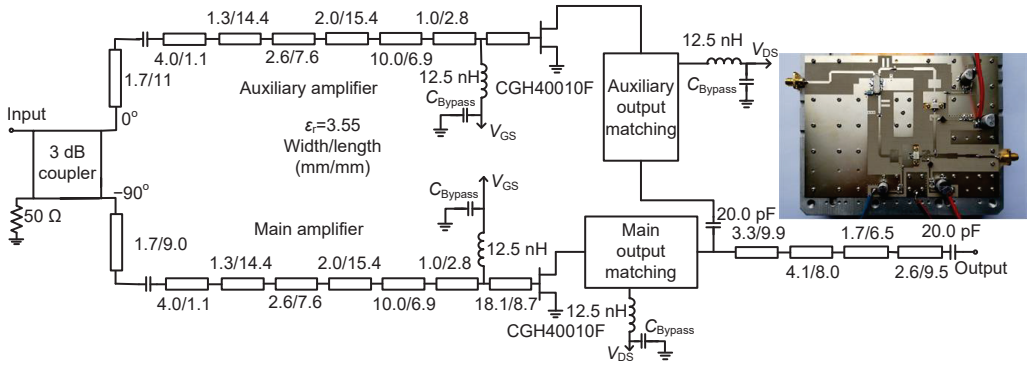

Fig. 7 Complete schematic of the proposed Doherty power amplifier (DPA) (Inset shows the fabricated DPA)

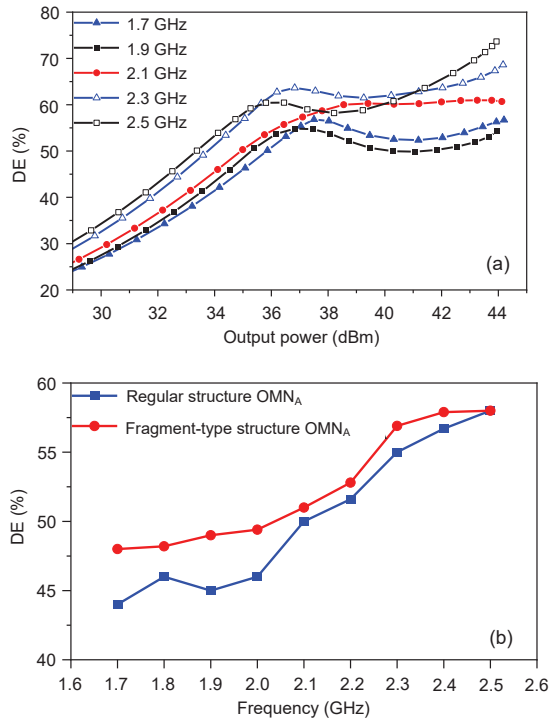

Fig. 8 Doherty power amplifier (DPA) simulation results: (a) drain efficiency (DE) and frequency vs. output power; (b) efficiency comparison of 9-dB back-off power (BOP)

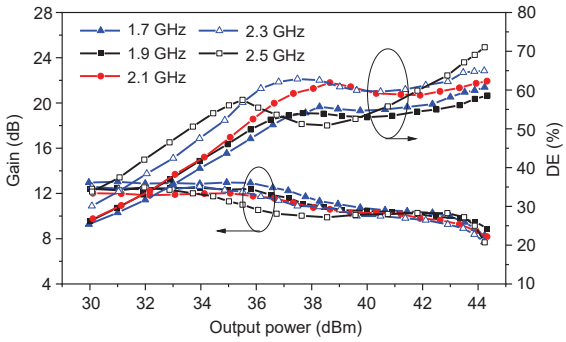

Fig. 9 Measurement results of the gain and drain efficiency (DE) for the proposed Doherty power amplifier (DPA)

4 Experimental results

For further verification, the designed DPA was fabricated, as depicted in Fig. 7. Fig. 9 illustrates the measurement results using continuous waves. It presents the measured efficiency and gain characteristics as the function of output power. From this figure, it can be noted that the DPA exhibits distinct Doherty operation characteristics within the operating frequency range, achieving high efficiency at 9-dB BOP. Fig. 10 presents the saturated output power, efficiency, and 9-dB BOP DE within the 1.7–2.5 GHz operating bandwidth. The saturated output power exceeds 44 dBm within the operating bandwidth, and the DE ranges within 58.5%–68% and 45%–55% at saturation and 9-dB BOP, respectively. The power added efficiency (PAE) in the saturation and 9-dB BOP is >50.8% and >43.2%, respectively. Measurement results indicate that the proposed method can enhance the consistency of BOP efficiency in the DPA using IER while achieving bandwidth expansion.

To validate the linearity of the power amplifier, digital pre-distortion (DPD) linearization measurements were conducted at 1.7, 2.1, and 2.5 GHz. The measurement was conducted at an average output power of approximately 35 dBm, using a 20-MHz long-term evolution (LTE) modulation signal with a PAPR of 8 dB. The results illustrated in Fig. 11 show that the designed DPA achieves an adjacent channel leakage ratio (ACLR) of <−50 dBc with an

average efficiency >50%.

Table 1 presents a performance comparison with some existing large BOP range DPAs. It can be concluded that the proposed DPA can achieve extended bandwidth while maintaining good efficiency at the 9-dB BOP range.

5 Conclusions

The present paper introduces an optimized method for the OMN design of the DPA using IER. An impedance–phase hybrid objective function in conjunction with a fragment-type structure was employed to mitigate the efficiency inconsistency caused by phase dispersion within the wideband range. Compared to conventional regular structure designs, the relative operating bandwidth of the optimized DPA can be expanded with high BOP efficiencies.

Contributors

Zhongpeng NI, Jing XIA, and Wa KONG designed the research. Zhongpeng NI drafted the paper. Xinyu ZHOU, Wence ZHANG, and Xiaowei ZHU helped organize the paper. Jing XIA revised and finalized the paper.

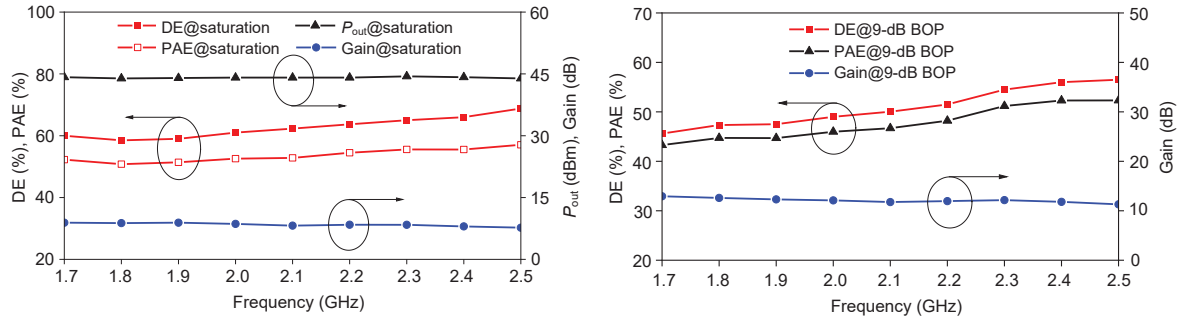

Fig. 10 Measurement results vs. frequency (DE: drain efficiency; PAE: power added efficiency)

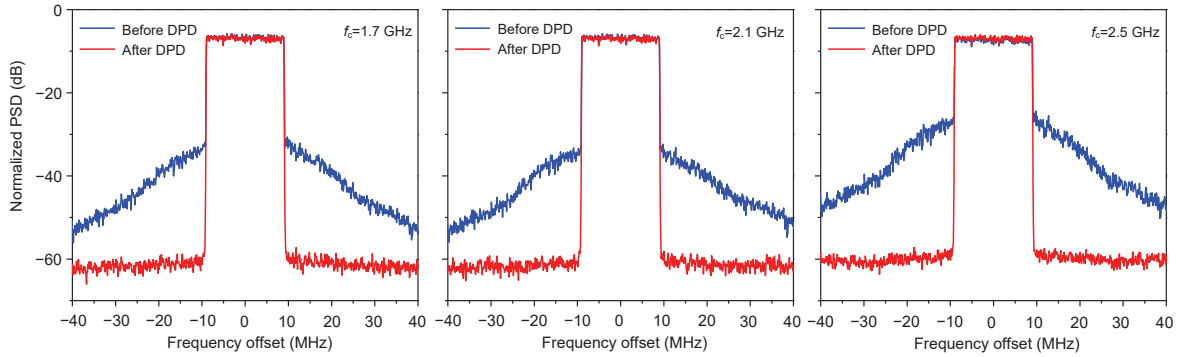

Fig. 11 Measured spectra before and after linearization for 20-MHz LTE modulation signal (LTE: long-term evolution; DPD: digital pre-distortion; PSD: power spectral density)

Table 1 Performance comparison of DPAs

Reference	Type	Frequency (GHz)	FBW (%)	DE@SAT (%)	BOP (dB)	DE@BOP (%)
Kong et al. (2018)	Sym.	2.2–2.5	12	63–68	9	45–52
Ruhul Hasin and Kitchen (2019)	Sym.	2.1–2.3	9	71	9	54
Li C et al. (2020)	Sym.	1.9–2.4	23	65.2–78	8.5–9	44.2–49.7
Guo et al. (2022)	Asym.	2.0–2.6	26	60.5–78	9	44.6–65
Li MY et al. (2023)	Asym.	1.6–2.1	27	47–62.7	12	42.2–52.1
Zhang JR et al. (2023)	Sym.	2.05–2.8	31	66–76	9	40–49
This work	Sym.	1.7–2.5	38	58.5–68	9	45–55

DPA: Doherty power amplifier; FBW: fractional bandwidth; DE: drain efficiency; SAT: saturation; BOP: back-off power; Sym.: symmetric; Asym.: asymmetric

Conflict of interest

All the authors declare that they have no conflict of interest.

Data availability

The data that support the findings of this study are available from the corresponding author upon reasonable request.

References

Akbarpour M, Helaoui M, Ghannouchi FM, 2012. A transformer-less load-modulated (TLLM) architecture for efficient wideband power amplifiers. *IEEE Trans Microw Theory Tech*, 60(9):2863-2874. https://doi.org/10.1109/TMTT.2012.2206050

Asbeck P, Popovic Z, 2016. ET comes of age: envelope tracking for higher-efficiency power amplifiers. *IEEE Microw Mag*, 17(3):16-25. https://doi.org/10.1109/MMM.2015.2505699

Chen SC, Wang WW, Xu KW, et al., 2018. A reactance compensated three-device Doherty power amplifier for bandwidth and back-off range extension. *Wirel Commun Mob Comput*, 2018:8418165. https://doi.org/10.1155/2018/8418165

Choi W, Kang H, Oh H, et al., 2021. Doherty power amplifier based on asymmetric cells with complex combining load. *IEEE Trans Microw Theory Tech*, 69(4):2336-2344. https://doi.org/10.1109/TMTT.2021.3059666

Chung A, Rejeb MB, Darwish A, et al., 2018. Frequency doubler based outphasing system for millimeter wave vector signal generation. Proc 15th European Radar Conf, p.449-452. https://doi.org/10.23919/EuRAD.2018.8546541

Cui J, Li PP, Sheng WX, 2023. High linearity U-band power amplifier design: a novel intermodulation point analysis method. *Front Inform Technol Electron Eng*, 24(1):176-186. https://doi.org/10.1631/FITEE.2200082

Dai ZJ, Kong SM, Feng W, et al., 2024. Design of wideband asymmetric Doherty power amplifier using a new phase compensation technique. *IEEE Trans Circ Syst I Regular Papers*, 71(3):1093-1104. https://doi.org/10.1109/TCSI.2023.3336558

Doherty WH, 1936. A new high efficiency power amplifier for modulated waves. *Proc Inst Radio Eng*, 24(9):1163-1182. https://doi.org/10.1109/JRPROC.1936.228468

Fang XH, Cheng KKM, 2014. Extension of high-efficiency range of Doherty amplifier by using complex combining load. *IEEE Trans Microw Theory Tech*, 62(9):2038-2047. https://doi.org/10.1109/TMTT.2014.2333713

Guo J, Crupi G, Cai JL, 2022. A broadband asymmetric Doherty power amplifier design based on multiobjective Bayesian optimization: theoretical and experimental validation. *IEEE Access*, 10:89823-89834. https://doi.org/10.1109/ACCESS.2022.3201348

Karahan EA, Liu Z, Sengupta K, 2023. Deep-learning-based inverse-designed millimeter-wave passives and power amplifiers. *IEEE J Sol-State Circ*, 58(11):3074-3088. https://doi.org/10.1109/JSSC.2023.3276315

Kong W, Xia J, Meng F, et al., 2018. A Doherty power amplifier with large back-off power range using integrated enhancing reactance. *Wirel Commun Mob Comput*, 2018:3968308. https://doi.org/10.1155/2018/3968308

Kong W, Zhong YJ, Xia J, et al., 2024. Optimization design of broadband Doherty PA using fragment-type matching network based on dual-state impedance objective function. *IEEE Trans Circ Syst II Express Briefs*, 71(4):1809-1813. https://doi.org/10.1109/TCSII.2023.3332178

Li C, You F, Peng J, et al., 2020. Co-design of matching sub-networks to realize broadband symmetrical Doherty with configurable back-off region. *IEEE Trans Circ Syst II Express Briefs*, 67(10):1730-1734. https://doi.org/10.1109/TCSII.2019.2946395

Li M, Li ZQ, Zheng Q, et al., 2022. A 17–26.5 GHz 42.5 dBm broadband and highly efficient gallium nitride power amplifier design. *Front Inform Technol Electron Eng*, 23(2):346-350. https://doi.org/10.1631/FITEE.2000513

Li MY, Cheng XB, Dai ZJ, et al., 2023. A novel method for extending the output power back-off range of an asymmetrical Doherty power amplifier. *Front Inform Technol Electron Eng*, 24(3):470-479. https://doi.org/10.1631/FITEE.2200250

Liu X, Lv GS, Wang DH, et al., 2020. Energy-efficient power amplifiers and linearization techniques for massive MIMO transmitters: a review. *Front Inform Technol Electron Eng*, 21(1):72-96. https://doi.org/10.1631/FITEE.1900467

Lyu H, Lovato R, Gowri SP, et al., 2023. Co-design of Doherty power amplifier and post-matching bandpass filter. IEEE Wireless and Microwave Technology Conf, p.65-68. https://doi.org/10.1109/wamicon57636.2023.10124924

Nan JC, Wang H, Cong MF, et al., 2021. A broadband Doherty power amplifier with a new load modulation network. *IEEE Access*, 9:58025-58033. https://doi.org/10.1109/ACCESS.2021.3072780

Özen M, Andersson K, Fager C, 2016. Symmetrical Doherty power amplifier with extended efficiency range. *IEEE Trans Microw Theory Tech*, 64(4):1273-1284. https://doi.org/10.1109/TMTT.2016.2529601

Pang JZ, He SB, Huang CY, et al., 2015. A post-matching Doherty power amplifier employing low-order impedance inverters for broadband applications. *IEEE Trans Microw Theory Tech*, 63(12):4061-4071. https://doi.org/10.1109/TMTT.2015.2495201

Ren M, Gao RB, Liu S, et al., 2024. Design of wideband Doherty power amplifier using inverse continuous class-F mode. *IEEE Trans Circ Syst II Express Briefs*, 71(9):4176-4180. https://doi.org/10.1109/TCSII.2024.3379992

Roychowdhury D, Kitchen J, 2022. Asymmetrical continuous mode Doherty power amplifier using complex combining load impedance. IEEE Texas Symp on Wireless and Microwave Circuits and Systems, p.1-5. https://doi.org/10.1109/WMCS55582.2022.9866245

Ruhul Hasin M, Kitchen J, 2019. Exploiting phase for extended efficiency range in symmetrical Doherty power amplifiers. *IEEE Trans Microw Theory Tech*, 67(8):3455-3463. https://doi.org/10.1109/TMTT.2019.2921366

Shi WM, He SB, Gideon N, 2017. Extending high-efficiency power range of symmetrical Doherty power amplifiers by taking advantage of peaking stage. *IET Microw Antenn Propag*, 11(9):1296-1302. https://doi.org/10.1049/iet-map.2017.0119

Shi WM, He SB, Zhu XY, et al., 2018. Broadband continuous-mode Doherty power amplifiers with non-infinity peaking impedance. *IEEE Trans Microw Theory Tech*, 66(2):1034-1046. https://doi.org/10.1109/TMTT.2017.2749224

Wang H, Nan JC, Cong MF, et al., 2022. A broadband power amplifier with multifrequency impedance matching. *IEEE Microw Wirel Compon Lett*, 32(11):1339-1342. https://doi.org/10.1109/LMWC.2022.3187998

Xia J, Yang MS, Guo Y, et al., 2016. A broadband high-efficiency Doherty power amplifier with integrated compensating reactance. *IEEE Trans Microw Theory Tech*, 64(7):2014-2024. https://doi.org/10.1109/TMTT.2016.2574861

Xia J, Bian CX, Kong W, et al., 2022. Optimization design of fragment-type filtering matching network for continuous inverse class-F power amplifier. *IEICE Electron Express*, 19(14):20220043. https://doi.org/10.1587/elex.19.20220043

Xiao F, Dai ZJ, Pang JZ, et al., 2021. A Doherty power amplifier with extended back-off by using non-infinite peaking impedance and complex combining load. IEEE MTT-S Int Microwave Workshop Series on Advanced Materials and Processes for RF and THz Applications, p.182-184. https://doi.org/10.1109/imws-amp53428.2021.9643873

Xu Y, Pang JZ, Wang XY, et al., 2021. Enhancing bandwidth and back-off range of Doherty power amplifier with modified load modulation network. *IEEE Trans Microw Theory Tech*, 69(4):2291-2303. https://doi.org/10.1109/TMTT.2021.3056402

Yang ZX, Yao Y, Li MY, et al., 2019. Bandwidth extension of Doherty power amplifier using complex combining load with noninfinity peaking impedance. *IEEE Trans Microw Theory Tech*, 67(2):765-777. https://doi.org/10.1109/TMTT.2018.2884415

Yao Y, Dai ZJ, Li MY, 2024. A novel topology with controllable wideband baseband impedance for power amplifiers. *Front Inform Technol Electron Eng*, 25(2):308-315. https://doi.org/10.1631/FITEE.2300074

Zhang JR, Zheng SY, Yang N, 2023. An efficient broadband symmetrical Doherty power amplifier with extended back-off range. *IEEE Trans Circ Syst II Express Briefs*, 70(4):1316-1320. https://doi.org/10.1109/TCSII.2022.3227045

Zhang QF, Li H, 2007. MOEA/D: a multiobjective evolutionary algorithm based on decomposition. *IEEE Trans Evol Comput*, 11(6):712-731. https://doi.org/10.1109/TEVC.2007.892759

Zhou H, Perez-Cisneros JR, Hesami S, et al., 2022. A generic theory for design of efficient three-stage Doherty power amplifiers. *IEEE Trans Microw Theory Tech*, 70(2):1242-1253. https://doi.org/10.1109/TMTT.2021.3126885

Zhou LH, Zhou XY, Chan WS, 2023. A compact and broadband Doherty power amplifier without post-matching network. *IEEE Trans Circ Syst II Express Briefs*, 70(3):919-923. https://doi.org/10.1109/TCSII.2022.3218006

Zhou XY, Chan WS, Sharma T, et al., 2022. A Doherty power amplifier with extended high-efficiency range using three-port harmonic injection network. *IEEE Trans Circ Syst I Regular Papers*, 69(7):2756-2766. https://doi.org/10.1109/TCSI.2022.3160382